Notes on a simple coagulation model — last update 4 January 2004

George A. Jackson
Texas A&M University
College Station, TX 77843, USA
gjackson@tamu.edu

January 4, 2005
simple_notes.tex

1 Introduction

This document is a quick introduction to the **simple** program and the theory behind it. The information on how to run the model is in first part of the document; the theory is later, in "Background" sections.

I have tried to be consistent in my notation, but do not guarantee that I have succeeded.

The complete calculation can be invoked inside the Matlab command window by simply typing `simple"`. This starts a script whose job is to call three other scripts, controlling the calculation of coagulation kernels (**simpbeta**), the solution of the dynamic coagulation equations (**simpcoag**), and the display of the results (**simpgraph**). This separation into three subprograms makes it simple to invoke only the dynamic differential equation solver without recalculating the kernels if the relevant parameters have not changed.

In order to simplify the use of the model, the programs interrogate the user on values for the important parameters. All of the parameters have default values which are set at the beginning of each program. The default values can be easily changed in the **matlab** editor. To accept the default values, simply press the "ENTER" key; to change a value, type in the new value, followed by the "ENTER" key.

The default values of the parameters are at the beginning of each script.

The model tracks the "conserved volume" (the non-water particle mass divided by density of the solid particle) in each section. The coagulation equations are solved using the sectional approximation. The results are the amount of conserved volume in each section as a function of time and can be used to

2 Matlab files used in these programs.

The following programs calculate the particle size spectrum that results from a dividing algal cell. It is written in Matlab 6. If you wish to run under Matlab 5, you will need to change the references to

"quadl" to "quad8" and change the use of function handles back to strings (*e.g.*, "ode45(@rate,x,y)" to "ode45(rate,x,y)").

The available software modules and their functions are:

simple.m: The master module, it calls the next three matlab scripts, **simpbeta.m**, **simpcoag.m**, and **simpgraph.m**. These scripts can be run on their own, as well as called by **simple**.

simpbeta.m This script calculates the betas used in the coagulation calculations. It can be run separately from the other scripts, but it requires the following functions:

simptcalc.m: (the controlling function)

betcds.m: curvilinear kernel for differential sedimentation

betcsh.m curvilinear kernel for shear

betrds.m rectilinear kernel for differential sedimentation

betrsh.m rectilinear kernel for shear

betfds.m fractal kernel for differential sedimentation

betfsh.m fractal kernel for shear

setvel.m the particle settling velocity as function of radius.

simpcoag.m: This script calculates the the evolution of the particle size spectrum via coagulation. It requires that the beta coefficients have been calculated by **simpbeta.m**. The default file for saving the result of **simpbeta** is **betaf.mat**, although others may be chosen. It also requires the functions

setvel.m the particle settling velocity)

simpcoagr.m the function making the rate calculations for the ode solver

finitial.m the function used to initialize the particle size spectrum.

simpgraph.m This script graphs the results. It requires that **simpcoag** have been run and the results saved as **simpout.mat**. It uses the utility

stamp.m put a time stamp in the upper right hand corner of figure.

2.1 Calculating the kernels: simpbeta.m

The three types of kernels are described in the background sections. The shear kernels are saved separately so that they can be varied in **simpcoag.m** without having to recalculate all the kernels.

Examples of the default constants set in **simpcoag.m** are :

```
                    %   setup the default constants

fr          = 2.33;                          % fractal dimension
dia0        = 20.8e-4;                       % unit particle diameter, cm
delrho      = (4.5*2.48)*visc*rhofl/grav* (dia0/2)^(-0.83); % excess density, g/cm^3
nsect       = 20;                            % number of sections to use
nkernel     = 3;                             % which kernel? rect-1; curv-2; frac-3
coutfile    = 'betaf';
```

2.2 Solving the differential equations: simpcoag.m

The equations being solved are fairly stiff. One indication that the differential equation solver is having problems is that some of the output concentrations are negative. This is usually not much of a problem, as it occurs for those particles where the concentrations are so low as to be hypothetical, but it is indicative of an accuracy problem. As a result, you should test the reproducibility of the results for different numerical conditions. A useful test is to decrease the time interval for output (`deltttim`). It is also useful to play with other differential equation solver used in matlab.

Examples of the default constants set in **simpcoag.m** are :

```
                % constants
                % the following are defaults
rt      = 3e-14;                        % relative and absolute tolerances
at      = 1e-16;
cbeta   = 'betaf';                      % default name of beta file
tfinal  = 21.;                          % start and end times
alpha   = 1;                            % set the stickiness to 0.8
Lz      = 65;                           % thickness of the layers(m)
Lgam    = 0.1;                          % average shear, 1/s
Lmu     = 0.15;                         % specific growth rate in first section, 1/d
num_1   = 35;                           % initial number of particles/cm^3 in first section
nsecgro = 3;                            % section at which stop growth in aggreg.
delttim = 0.25;                         % time interval between output, affects acc, d
```

2.3 Graphical output: simpgraph.m

simpgraph.m generates 2 and 3-dimensional plots of the results. The choice of one or the other is the only choice offered.

The 2-dimensional case provides different ways of looking at the results (Fig. 1). The left hand side has the number spectrum $n(r)$ (top, left) and the mass (volume) flux spectrum nVv (bottom,left), where V is the particle volume and v is its settling speed. Each line represents the results for a different time, with the time interval set in **simpcoag.m**. The middle two graphs show the results for each section in time. Each line represents a different section, with the smaller particles usually having the higher concentrations. The top line, indicated by plus signs, is the sum of all sections. Shown are the sectional concentrations Q_i (top, middle), and fluxes $Q_i v$ (bottom, middle). Also shown is the average velocity, calculated as the total particle flux divided by the total mass. It decreases initially as large particles fall out without being replaced; it increases when coagulation starts to form larger particles.

Figure 1: Output from simple model run, with 2 dimensional option (default).

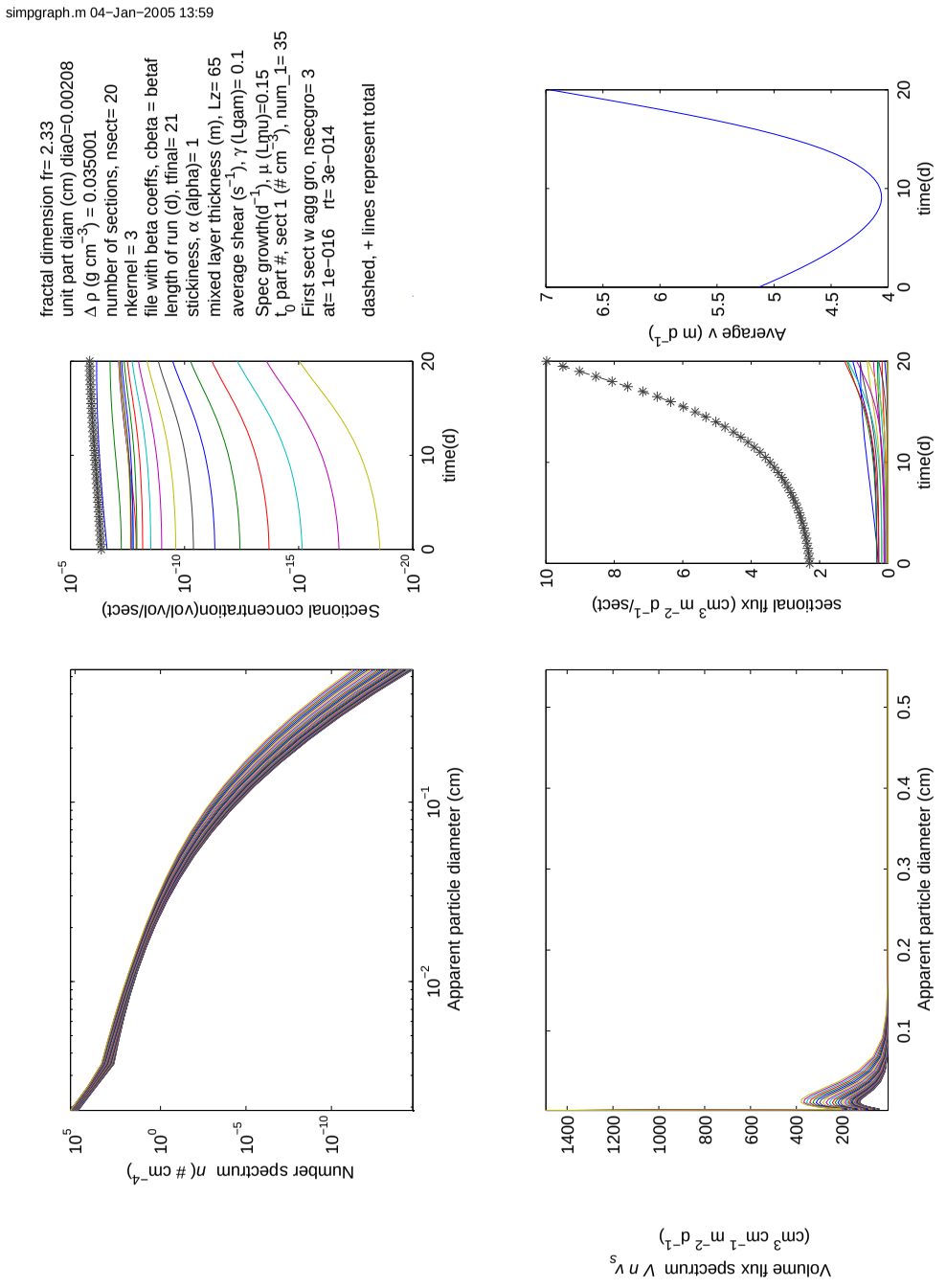

The 3-dimensional case also provides different ways of looking at the results (Fig. 2). Shown are the mass (volume) flux spectrum (top, left), number spectrum (bottom, left), and the mass (volume) spectrum nV (middle, lower) as functions of time and diameter. Also shown is sectional concentrations in time (top, middle).

Figure 2: Output from simple model run, with 3 dimensional option.

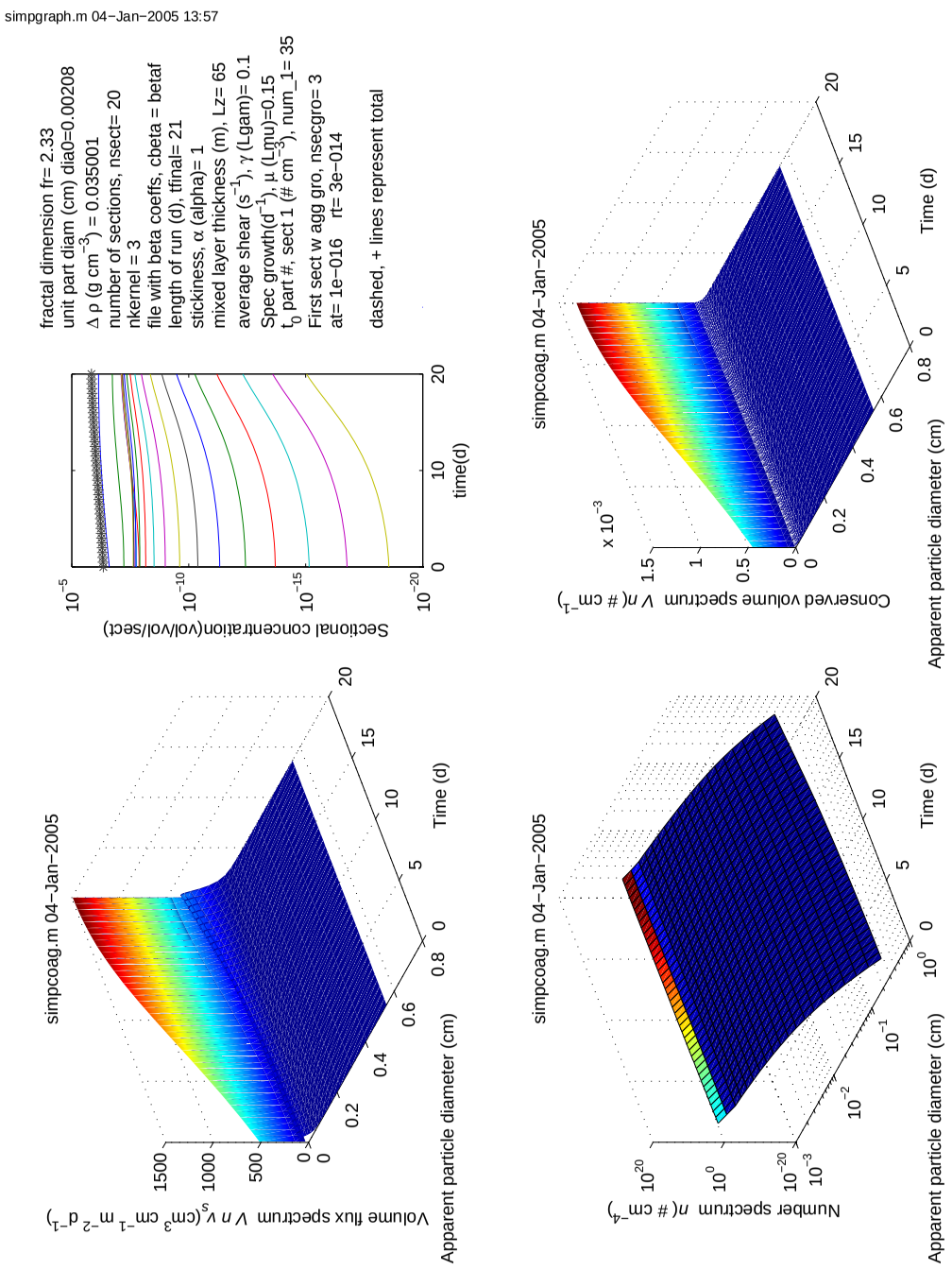

In both cases, the values of the model parameters are printed in the upper right-hand corner of the plots.

3 Background: background

A large group of problems revolve around the contact between two organisms or particles. Such problems can be broken into two parts: determining the approach distance at which the particles can interact and determining the rates at which the two particles come within this distance.

Two particles/organisms can be brought together as a result of differential water motion, such as by turbulence, as a result of directed motion, such as swimming in one direction or settling, or as a result of random motions. The analysis of such mechanisms is similar for organisms and for particles, although the details vary. The theory for particle interactions is more refined by a more detailed description of the hydrodynamics and surface forces than that of organism interactions.

4 Background: the particle size spectrum

Fundamental to the description of particle concentrations is the particle number spectrum. If N is the cumulative particle concentration, the total number of particles per unit volume larger than a given size, then $n = -\frac{dN}{dd}$ is the particle number spectrum, here expressed as the rate of change of N with respect to particle diameter d. n can also be expressed in terms of other measures of particle size, including particle mass ($n_m = -\frac{dN}{dm} = n \cdot \frac{dd}{dm}$) and volume. It allows the description of particle concentration as a function of size when particle sizes vary continuously, much as light spectra allow the description of a photon flux that varies with wavelength. The number of particles per unit volume with radii between r and $r + dr$ is given by $n(r)dr$, where $n(r)$ is the particle size spectra.

Spectral graphs with a large range for the diameters are frequently plotted with the x-axis representing the logarithm of the diameter. This spreads out the fraction of the figure occupied by the small diameters, suggesting that they are more important than they are. Here importance is the area under the curve for a range of diameters. In this case, we would like to have the number of particles be proportional to the area under the curve for that range. This works if the x-axis is linearly related to the diameter but not if it is related to the logarithm. How de we handle this problem? What we would for this case is to plot $\frac{-dN}{d\log \text{diameter}}$ as a function of log diameter. However, d_p is the particle diameter

$$\frac{-dN}{d\log d_p} = \frac{-dN}{dd_p}\frac{dd_p}{d\log d_p} = n\frac{dd_p}{d\log d_P} = nd_p \tag{1}$$

As a result, if we weight n by multiplying the particle diameter (or radius or mass) we can force the area under the curve to be proportional to the number of particles within the size range.

Particle size spectra typically show much greater values at small sizes than at large. They typically are power law functions of particle diameter for large ranges

$$n = ad^{-b} \tag{2}$$

where d is the particle diameter and a and b are constants. If $b = 4$, the spectrum is considered to follow the *Junge power law* (*e.g.*, Pruppacher and Klett, 1980). Such a spectrum has equal particle volumes in equal logarithmic size intervals.

One of the reasons for working with the number spectrum is that it is an extremely powerful tool. If I want to know the total volume of particles within a diameter range of d and $d + dd$, where dd is an infinitesmal diameter increment, I simply multiply the volume of one particle $V(d)$ by the number spectrum $n(d)$ and the interval dd. It is not much use to know what is happening in an infintesmal interval. If we want to know the particle volume within a range of d_l and d_u, we integrate:

$$\text{total particulate volume} = \int_{d_l}^{d_u} V\ n\ dd \tag{3}$$

Figure 3: Particle size spectrum for Monterey Bay on 29 July 1993 at 10 m. The different lines denote the results from different instruments. The results have been transformed to the photographic-image equivalent diameters. The dotted line represents the least-squares fit to the log transformed data. Jackson *et al.*(1997)

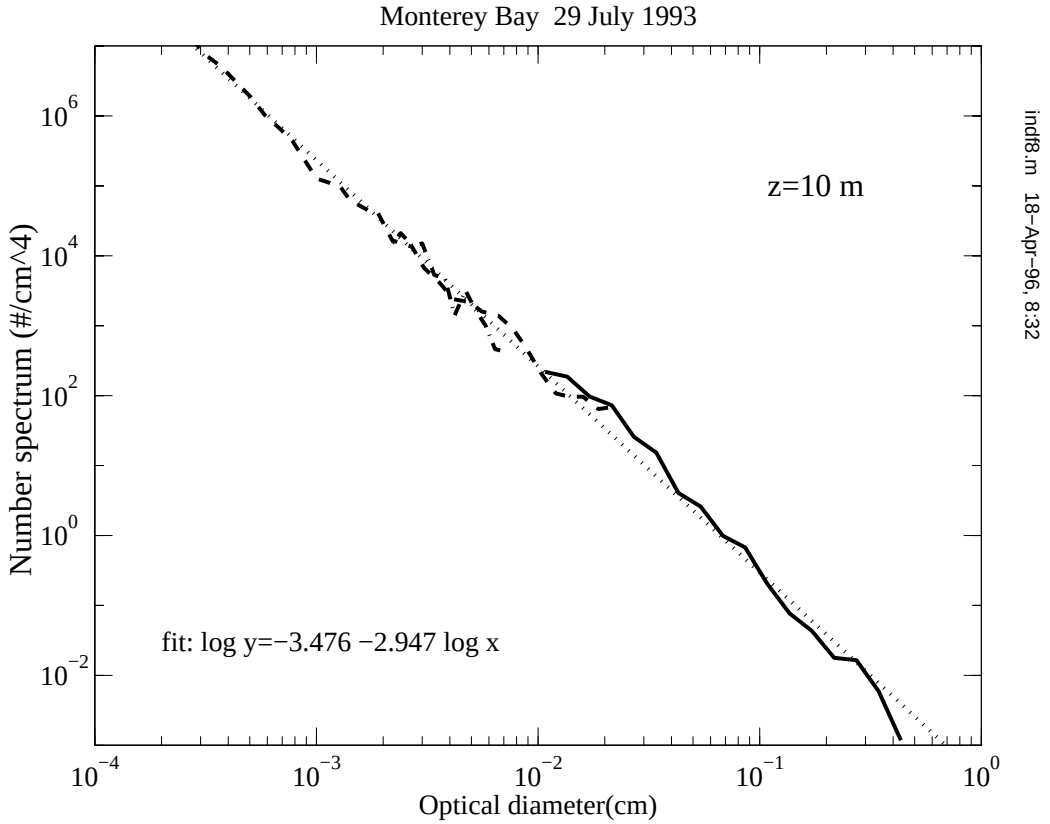

One can calculate the amount of any quantity, including particle volume, surface area, carbon mass, number, ..., as long as one knows the quantity in a single particle as a function of particle size and the number spectrum.

There are a few tricks to worry about. First, fractal scaling (Eq. 22) means that the power law fit that one obtains depends on what sort of instrument was used to size the particles. For example, a Coulter Counter measures a quantity close to the conserved particle mass (that without the enclosed water). As a result, the diameter calculated using the data from one is close to the *conserved volume equivalent*. The diameter measured from an image of the particles is more akin to the fractal diameter. Because the ratio of the two diameters changes as the particles become bigger, the power law fits differ between the two. Furthermore, the particle mass is not proportional to the image diameter cubed. While such effects can be compensated for, they must be included.

Second, because the particle sizes and the spectral values usually studied vary over such large ranges, the results are usually presented in a log-log plot. Such curves can be deceptive. For example, I can calculate a volume spectrum as $v_{sp} = n(d) \cdot V(d)$. When I plot $\log v_{sp}$ versus $\log d$, it looks as if most

Figure 4: Particle mass distribution for Monterey Bay on 29 July 1993 at 10 m. The area under a curve is proportional to the particle mass in its size range because of the scaling of the y-axis. Notice that most of the particle mass in the larger particles ($d > 100$ μm). This can be ascribed to coagulation of small particles into larger ones, but with the largest particles being broken apart by water shear. Jackson *et al.*(1997)

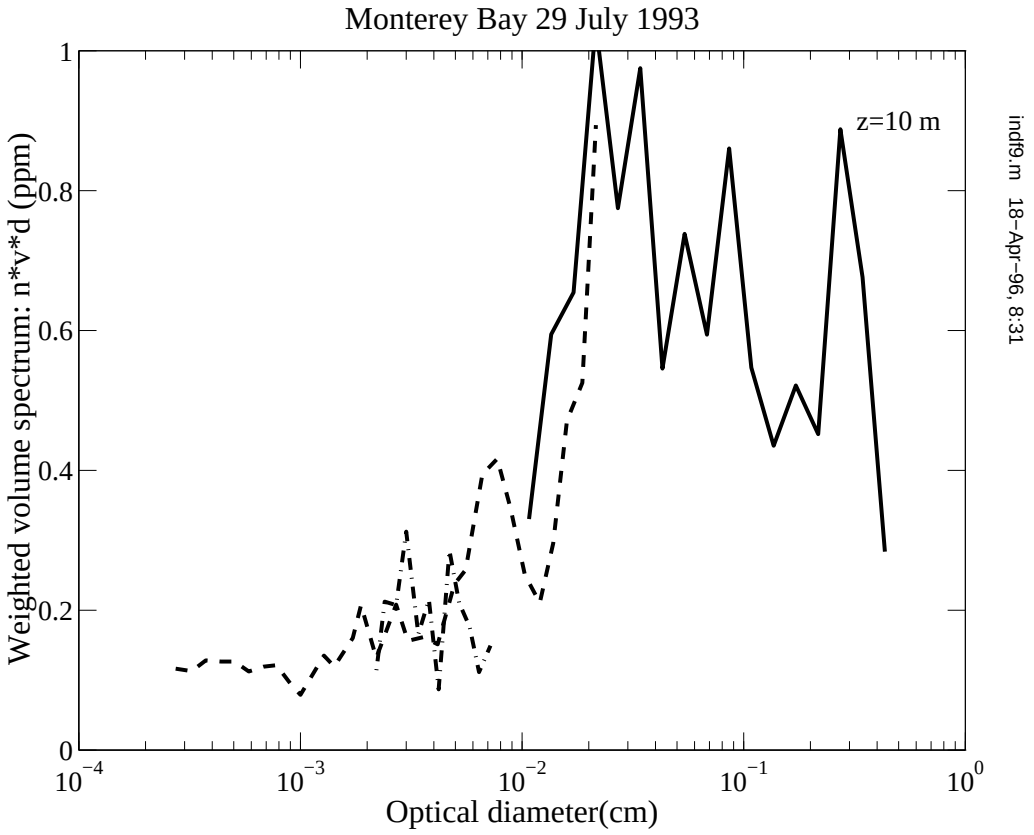

of the volume is in the small particles because we tend to associate the area under the curve with the total volume. We need to change this. If V_T is the equivalent of N, then the total volume concentration is

$$V_T = \int_{d_l}^{d_u} v_{sp} dd = \int_{\ln d_l}^{\ln d_u} v_{sp} d \; d(\ln d) = \log(e) \int_{\log d_l}^{\log d_u} v_{sp} d \; d(\log d) \tag{4}$$

where $d \ln d = d^{-1} dd$, or $dd = dd \ln d$ and $\log_{10} d = \log_{10}(e) \cdot \ln d$. Notice that the final integral is the area under the curve when we plot dnV as a function of $\log d$.

5 Background: coagulation mechanisms and resulting kernels

Physical coagulation theory distinguishes between collision and sticking of two particles. It treats the collision rates as being calculable for different mechanism. Sticking is usually treated as a probability

that is determined by chemistry and which can be described with a single value. The theory has been developed to describe the formation of rain drops from fog and the formation of smog (*e.g.*, Friedlander, 1977; Pruppacher and Klett, 1980). It has been applied to describe removal of particles in water treatment plants, colloids in rivers that hit the ocean, and formation of marine snow (*e.g.*, Jackson, 1990; O'Melia, 1972).

The key to the theory is to discover mechanisms that bring particles together and then describe their dynamics, which has been done to different levels of sophistication. There are three primary mechanisms usually invoked: differential sedimentation, Brownian motion, and shear (laminar and turbulent).

5.1 Differential sedimentation

Consider an organism swimming along at speed of v. If it comes into contact with every particle that is within R of it and if those other particles are present at a concentration of C, then

$$\text{Contact rate} = \pi R^2 v C \tag{5}$$

This is equivalent to stating that the organism is sweeping out a cylinder R wide as it swims. This concept is the basis of models for particles colliding as a result of different swimming or fall velocities.

The coagulation mechanism of differential sedimentation considers the interaction between two particles, of types i and j, falling at velocities v_i and v_j, having radii r_i and r_j, and present at concentrations C_i and C_j. We can consider their interactions at several levels of sophistication, depending on how much of the fluid dynamics and the surface attraction that we consider. We will start by considering the minimal model, in which we know that particle i falls faster than particle j but do not consider any other fluid dynamics. In this case, any (spherical) particle whose center is within $R = r_i + r_j$ of the centerline of the faster falling particle can contact it. This value for R is that at which the particles just touch when they are lined up at the same depth (Fig. 5). Then the relevant rate at which a given particle of i contacts j particles is given by Eq. 5, as

$$\text{Contact rate with one } i \text{ particle} = \pi(r_i + r_j)^2 (v_i - v_j) C_j$$

where the relevant velocity is now the difference between v_1 and v_2. The total contact rate per unit volume is the product of this and the C_i:

$$\begin{aligned} \text{contact rate per vol.} &= \pi(r_i + r_j)^2 (v_i - v_j) C_i C_j \\ &= \beta_{DS,ij} C_i C_j \qquad (6) \\ \text{where} & \\ \beta_{DS,ij} &= \pi(r_i + r_j)^2 |v_i - v_j| \qquad (7) \end{aligned}$$

where $\beta_{DS,ij}$ is known by several names, including the coagulation kernel for differential sedimentation. By using $|v_i - v_j|$ rather than $(v_i - v_j)$ we have made the formula apply regardless of which particle falls faster. Note that its size depends acutely on the sizes of the interacting particles. This version is known as the *rectilinear* version. It does not include any fluid dynamical effects. Among its properties is that if i is the larger particle, the contact rate depends mostly on r_i^2, proportional to the cross-sectional area of the larger particle.

If we start to worry about the fluid dynamics the situation changes. If we use the Stokes flow equations to derive the flow field around the larger of the two particles, in what is known as the *curvilinear* value, we get a much different result:

$$\beta_{DS,ij} = 0.5\pi r_j^2 \qquad \text{where } r_i >> r_j \tag{8}$$

Notice that the relationship now depends on the cross-sectional area of the *smaller* particle.

Figure 5: Collision from differential sedimentation. Shown are the collision cross-section for the rectilinear case, where the radius of the interaction cylinder equals the sum of the radii of the two particles, and the curvilinear case, where the smaller particle is assumed to follow the streamlines of fluid flow as it moves around the larger particle.

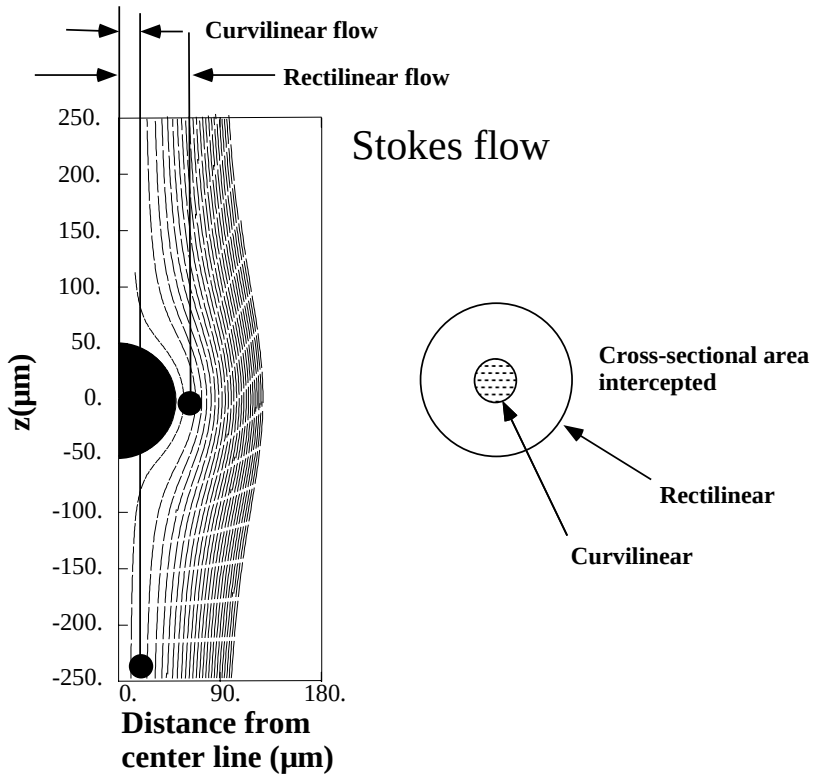

5.1.1 Other considerations

Most particles in the ocean are not spheres. Furthermore, the important class of particles known as aggregates are porous and should have some flow going through them as well as around. In either case, the above equations provide only an approximation to what is occurring in the ocean.

At the very small scales $\sim 5 - 10$ nm, other forces affect the relevant movement of particles. Most particles in seawater have negative charges (*e.g.*, Stumm and Morgan, 1995). The similar charges cause a repulsion between particles that is more important in fresh water than in salt water, where the many ions act to shield the charge effects. Other forces include induced dipole forces known as van der Waals forces.

5.2 Shear

Shear flow is fluid flow in which the water velocity changes with position. Simple shear is described by equations of the form $u_x = \gamma y$, $u_y = u_z = 0$, where u_x, u_y, and u_z are the fluid velocity components in the x, y, and z directions and γ is the shear gradient (Fig. 8).

Figure 6: Rectilinear coagulation kernels. A: total $\beta(r_i, r_j)$, calculated as the sum of $\beta_{Br}(r_i, r_j)$, $\beta_{ds}(r_i, r_j)$, and $\beta_{sh}(r_i, r_j)$. B: $\beta_{Br}(r_i, r_j)$, calculated for $T = 300$K, $\mu = 0.01$ poise. C:$\beta_{sh}(r_i, r_j)$ calculated for a shear of 1 s^{-1}; D: $\beta_{ds}(r_i, r_j)$ calculated for a constant particle density (fractal dimension = 3), $\Delta\rho = 0.05$ g cm^{-3}. The tick marks for radius are at 10^{-5}, 10^{-4}, 10^{-3}, 10^{-2}, and 10^{-1} cm.

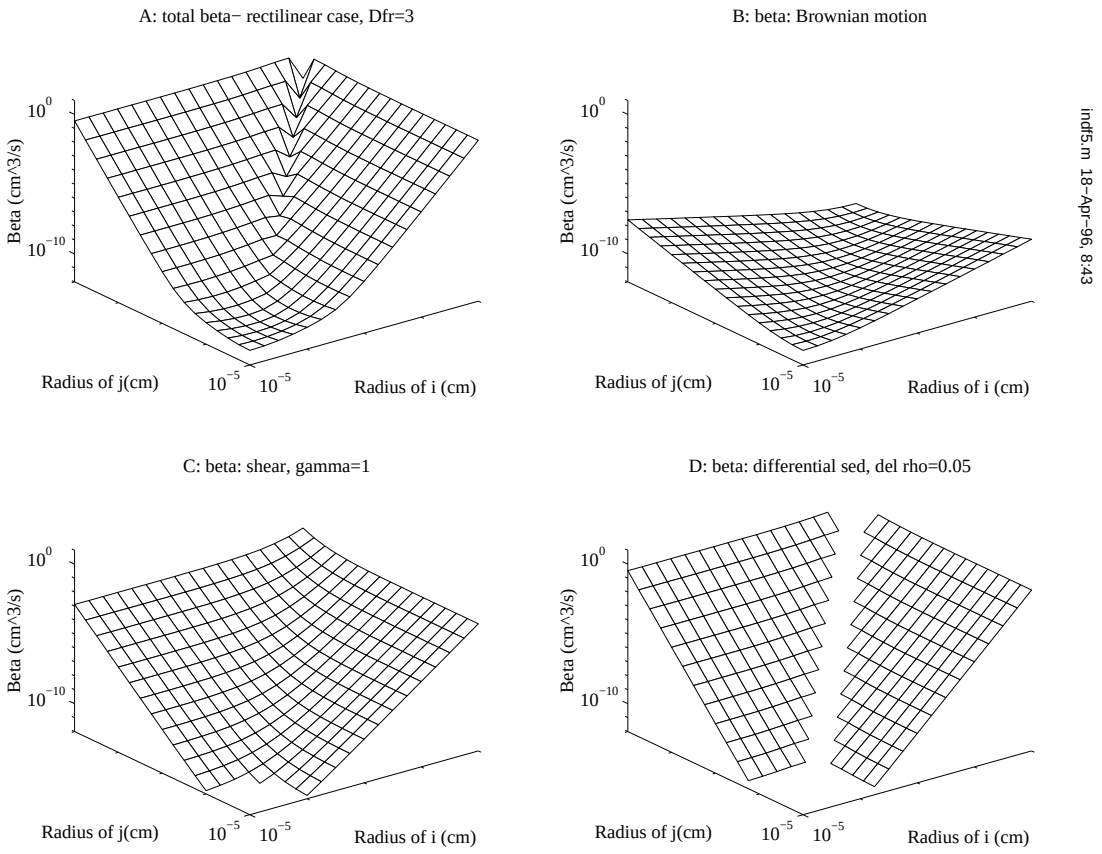

If we want to calculate the rate at which particles of radius r_j collide with particles of radius r_i, we have an added complication over the case of differential sedimentation. We anticipate that any particle whose center is within $R = r_i + r_j = (y^2 + z^2)^{0.5}$ of the x-axis will collide with particle 1 (Fig. 9). The problem is that the flow varies with y. To calculate the rate of collision for all such particles, we will double the capture rate for particles arriving with $0 < z < (r_i + r_j)$. We start by calculating the flux at any position:

$$\text{flux} = (\gamma z) C_j \tag{9}$$

where C_j is the concentration of particles of type 2. Next we sum up the contributions from all the points in the target region (=2 times that for the $z > 0$ region) by integrating the fluxes:

$$\text{flow} \quad = \quad 2 \int_0^R \int_{-y_c(z)}^{+y_c(z)} (\gamma z) C_j \, dy dz$$

Figure 7: Curvilinear coagulation kernels. A: total $\beta(r_i, r_j)$, calculated as the sum of $\beta_{Br}(r_i, r_j)$, $\beta_{ds}(r_i, r_j)$, and $\beta_{sh}(r_i, r_j)$. B: $\beta_{Br}(r_i, r_j)$, calculated for $T = 300$K, $\mu = 0.01$ poise. C:$\beta_{sh}(r_i, r_j)$ calculated for a shear of 1 s^{-1}; D: $\beta_{ds}(r_i, r_j)$ calculated for a constant particle density (fractal dimension = 3), $\Delta\rho = 0.05$ g cm^{-3}.

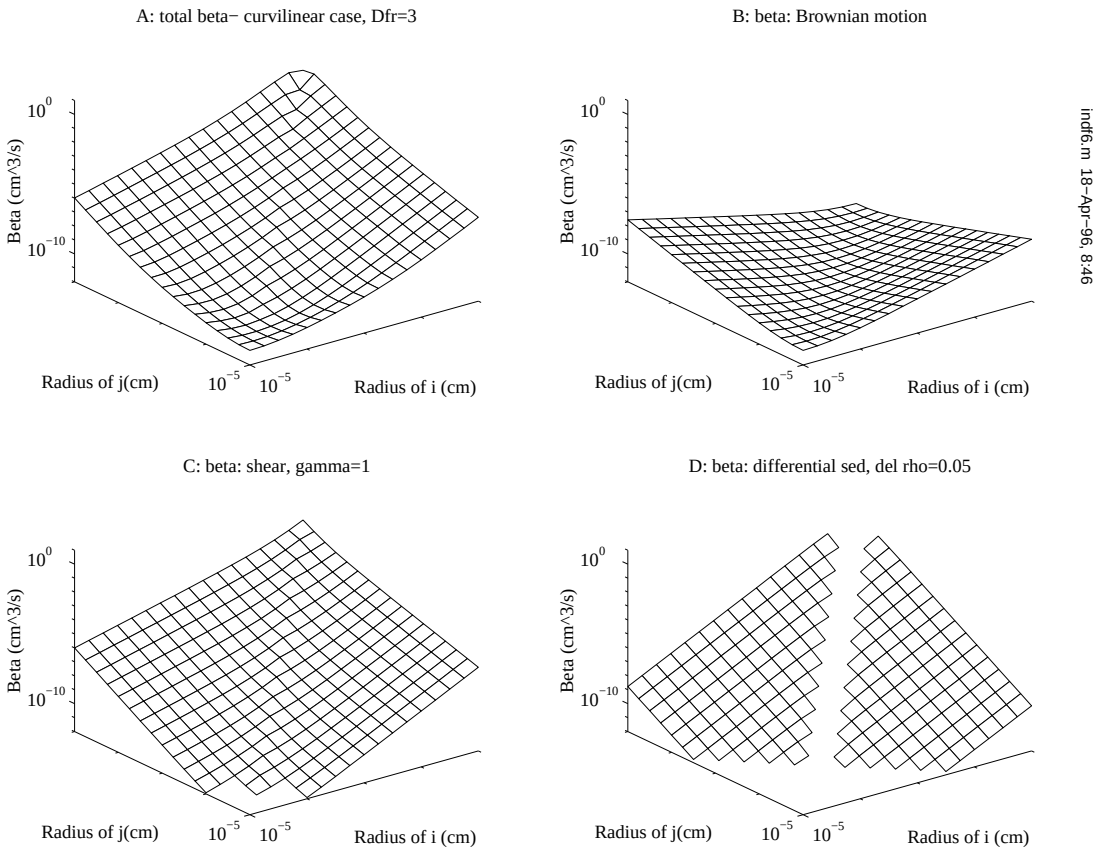

$$
\begin{aligned}
&= 4C_j\gamma \int_0^R z y_c(z) dz \\
&= 4C_j\gamma \int_0^{\pi/2} R\sin\theta\cos^2\theta d\theta \\
&= 4C_j\gamma R^3(-1) \int_i^0 \alpha^2 d\alpha \\
&= \frac{4}{3}\gamma(r_i + r_j)^3 C_j \\
&= \beta_{sh,ij} C_j
\end{aligned} \tag{10}
$$

Figure 8: Collision from shear. The arrows indicate the fluid velocities for uniform shear. The two particles are swept along towards a collision at a rate that depends on the separation distance and the shear rate. Collisions from Brownian motion tends to be more frequent for particles less than about 1 μm.

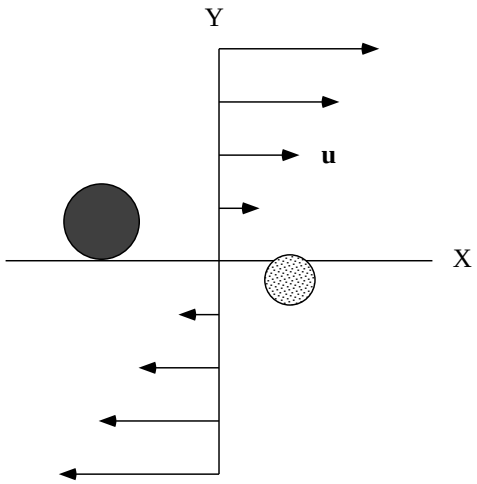

Figure 9: Geometry for shear. Left: the area of interaction. Any particle of radius r_j coming within a distance $R = r_i + r_j$ of particle i with radius r_i will be captured. Right: the coordinate system used to calculate the collision rate. y_c and z_c are the coordinates of the interaction circle in terms of radius R and angle θ.

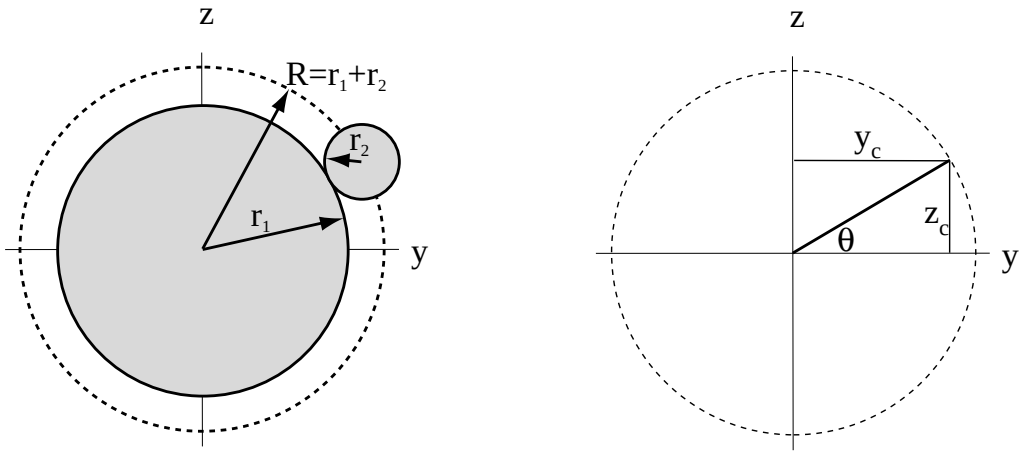

where $\theta = \sin^{-1}\frac{z}{R}$ (Fig. 9), $y_c = R\cos\theta$ is the y component of the interception circle, $\alpha = \cos\theta$, and

$$\beta_{sh,ij} = \frac{4}{3}\gamma(r_i + r_j)^3 \tag{11}$$

This is the rectilinear version of the laminar shear kernel.

The flow around a single particle in shear flow has been solved and applied to calculating the curvilinear version of β_{sh}. Values for β_{sh} have also been calculated for the flow between two interacting spheres and for the particle trajectories when molecular forces are included (*e.g.*, , Kao *et al.*, 1977; Batchelor and Green, 1972; Adler, 1981; Poe and Acrivos, 1975; Han, 1989) Because the results are too complicated to present analytically, they are usually presented in graphical or tabular form. One conclusion is that the water entrained by a particle acts as a significant barrier to contact between it and a smaller particle. Although this can be partially overcome by the attraction of van der Waals forces between the particles, there is still a substantial decrease in the contact rate when the radius of the smaller particle is less than 10% of the radius of the larger one.

Much of the interest in shear flow is the result of it being the manifestation of turbulent flow in the smallest, viscous, size range. For turbulent shear, the rectilinear coagulation kernel becomes (Saffman and Turner, 1956)

$$\beta_{sh,ij} = 1.3 \left(\frac{\epsilon}{\nu}\right)^{0.5} (r_i + r_j)^3 \tag{12}$$

where ϵ is the turbulent energy dissipation rate and ν is the kinematic viscosity of the fluid. If γ is estimated as $(\epsilon/\nu)^{0.5}$, the two equations are the same. The curvilinear version of this is

$$\beta_{sh,ij} = 10 \left(\frac{\epsilon}{\nu}\right)^{0.5} (r_i + r_j)^2 r_i \tag{13}$$

where $r_i << r_j$ (Hill, 1992).

Most calculations assume that particles are smaller than the Kolmogorov length. Delichatsios and Probstein (1975) argued for a different collision rate for larger particles. Hill et al.(1995) examined the effect experimentally...

5.3 Brownian motion

Put 10 particles next to a wall. In the absence of motion, nothing happens. If they are small they start to hop in what is known as *Brownian motion* and which is a manifestation of their diffusion. As they hop, they start to hit the wall. They can just as easily hit each other.

The diffusion coefficient for Brownian motion D is given by

$$D = \frac{kT}{6\pi\mu r} \tag{14}$$

where $k = 1.38 \times 10^{-23}$ J K^{-1} $= 1.38 \times 10^{-16}$ g cm^2 s^{-2} K^{-1} is the Boltzmann constant, T is the absolute temperature in K^{-1}, μ is the dynamic viscosity, and r is the particle radius. For $r = 0.5$ μm, the size of a small alga or a bacterium, $D = 4 \times 10^{-9}$ cm^2 s^{-1}. Remember that the typical chemical diffusivity is 10^{-5} cm^2 s^{-1}. Does this make sense? A typical molecule is about 10 nm across, equivalent to 0.001 of the bacterial cell. The above equation implies that the molecular diffusivity should be 1/0.001 times that of the bacterial cell, or about $4 \times 10^{-6} \sim 10^{-5}$ cm^2 s^{-1}. The numbers agree.

The probability that two particles will collide depends on their sizes and their diffusivities. In order to describe the rate at which two such particles collide, we need to be able to describe their relative diffusivities for two diffusing particles. Using the brackets <> to designate the average over all possible states, and $\mathbf{\Delta r}$ to describe the change in position of a particle over a period Δt, then from our previous work we know that

$$< \mathbf{\Delta r} >= 0$$

because the *average* position of a diffusing object (without a bias) is 0. Similarly, we describe the change over a time Δt in terms of the variance,

$$< |\mathbf{\Delta r}|^2 >=< \mathbf{\Delta r} \cdot \mathbf{\Delta r} >= 6D\Delta t$$

We are interested in how two particles, denoted 1 and 2, drift away from each other. Which is to say, we are interested in the distance between them:

$$\begin{aligned} < |\mathbf{\Delta r_1} - \mathbf{\Delta r_2}|^2 > &= < (\mathbf{\Delta r_1} - \mathbf{\Delta r_2}) \cdot (\mathbf{\Delta r_1} - \mathbf{\Delta r_2}) > \\ &= < |\mathbf{\Delta r_1}|^2 - 2\mathbf{\Delta r_1} \cdot \mathbf{\Delta r_2} + |\mathbf{\Delta r_2}|^2 > \\ &= < |\mathbf{\Delta r_1}|^2 > + < |\mathbf{\Delta r_1}|^2 > -2 < \mathbf{\Delta r_1} \cdot \mathbf{\Delta r_2} > \\ &= 6D_1\Delta t + 6D_2\Delta t + 0 \\ &= 6D_{12}\Delta t \end{aligned}$$

where $< \mathbf{\Delta r_1} \cdot \mathbf{\Delta r_2} >= 0$ if the motions of the two particles are uncorrelated and where $D_{12} = D_1 + D_2$.

We can write the rate at which particles of type j will collide with a particle of type i as as the solution for diffusion flow to a sphere of radius of $r_1 + r_2$ and and a diffusion coefficient D_{12}

$$\begin{aligned} \text{Flow rate to } i &= 4\pi(D_i + D_j)(r_i + r_j)C_j \\ &= \beta_{\mathrm{Br},ij} C_j \end{aligned} \tag{15}$$

where the subscripts refer to the properties of the two particles, C_j is the concentration of particle j, and $\beta_{\mathrm{Br},ij} = 4\pi(D_i + D_j)(r_i + r_j)$ is the *coagulation kernel* for Brownian motion. This is a modified version of the formula we developed for the flow of molecules to a sphere with the diffusivity and radius modified to account for mutual diffusion and combined particle size. If particle i is much larger than the particles of class j, Eq. 15 reduces to the equation describing diffusive flow to a sphere.

Eq. 15 gives the rate at which particles of group j collide with a single particle of group i. The rate at which such collisions occur in a unit volume is the number of i particles in the volume (C_i) times the above collision rate with the single particle:

$$\text{Collision rate per volume} = \beta_{\mathrm{Br},ij} C_i C_j \tag{16}$$

5.4 Effect of porous particles: the "fractal" kernels

Li and Logan (1997, 1997a) have experimentally determined the interaction rates between small, solid particles and larger aggregates, observing collision rates between those predicted by rectilinear and curvilinear kernels. They fit their results to curves which do not extrapolate well to the size range where both particles are the same size and where the differences between the curvilinear and rectilinear formulations are small. We have, therefore, modified the coagulation kernel to fit their observations but also to converge to the rectilinear solution when the particles are equal sized (Jackson, 2001).

For shear, this fractal kernel is

$$\beta_{sh-f,ij} = p^{0.88} \beta_{sh-r,ij} \tag{17}$$

where, again, p is the ratio of radii for small and large particles. This formulation also works well to describe the results of Serra and Logan (1999).

where $p = r_i/r_j$ and again $r_j \geq r_i$

For differential sedimentation, this fractal kernel is

$$\beta'_{ds-f,ij} = p^{0.984} \beta_{ds-r,ij} \tag{18}$$

5.5 Multiple mechanisms

While we tend to think of the above mechanisms as occurring independently, they do not necessarily do so. For example, the particle translation (differential sedimentation) can be enhanced by diffusion motions. To handle such situations, we appeal to dimensional parameters, such as the Peclet number, to calculate the increased transport.

5.6 Sticking of colliding particles

An important component of the coagulation process is the sticking of particles that collide. Kiørboe *et al.* (1990) estimated the value of α for several different phytoplankton species during different stages of nutrient limited growth in cultures and observed changes in algal stickiness. Alldredge *et al.* (1993) have observed that algal stickiness is also related to the presence of transparent particulate matter ("TEP"). This observation has been confirmed by Kiørboe *et al.* (1993). How to interpret these observations is not yet clear (*e.g.*, Jackson, 1995; Logan *et al.* 1995).

6 Background: coagulation theory

6.0.1 The kinetic coagulation equations

Coagulation models can be formulated assuming a monodisperse system, in which all of the particles are initially the same, or assuming a continuous size-distribution (Pruppacher and Klett, 1980; O'Melia, 1972). For the monodisperse case, an aggregate is composed of an integral number of monomers. The size class of a particle is denoted by a subscript which equals the number of monomers that it contains. Thus, r_i denotes the radius of a particle containing i monomers. In the continuous version, the radius could be an explicit function of the mass m: $r(m)$. Some formulations use the particle volume v as the master variable rather than mass. This approach is useful when volume is conserved and, hence, particle density is constant.

Classic coagulation models emphasize three mechanisms for particle-particle contact: Brownian diffusion, laminar and turbulent shear, and differential sedimentation. For each of these, the rate R_{ij} of forming new particles of mass $m_i + m_j$ from the collision of two smaller particles of masses m_i and m_j is given in terms of the number concentrations of the two colliding particles n_i and n_j, a rate constant called the coagulation kernel β_{ij}, and an efficiency factor E_{ij}:

$$R_{ij} = E_{ij} n_i n_j \beta_{ij} \tag{19}$$

In the absence of any non-aggregation processes, the rate of change in the concentration of a given particle size equals the sum of all rates from reactions that create that size particle less the sum from all those reactions that consume them (Pruppacher and Klett, 1980; O'Melia, 1972):

$$\frac{dn_i}{dt} = 0.5 \sum_{j=1}^{i} E_{j,i-j} \beta_{j,i-j} n_j n_{i-j} - n_i \sum_{j=1}^{\infty} E_{i,j} \beta_{i,j} n_j \tag{20}$$

For the case of continuous particle size distributions,

$$\begin{aligned} \frac{dn(m)}{dt} &= 0.5 \int_0^m E(m-m', m') \beta(m-m', m') n(m-m') n(m') dm' \\ &\quad - n(m) \int_0^\infty E(m, m') \beta(m, m') n(m') dm' \end{aligned} \tag{21}$$

6.0.2 Aggregates as fractals

Early coagulation models assumed that all particles were spheres of constant density. This is equivalent to assuming that volume, as well as mass, is conserved when two particles aggregate. Recent work, both theoretical and experimental, has shown that the particles formed by aggregation processes are often fractals, having fractal dimensions < 3 (Witten and Cates, 1986; Meakin 1991). Thus, the fraction of

fluid medium incorporated within the particle structure increases with the size of the particle. The resulting relationship between mass and length l of the aggregate can be expressed using the fractal dimension D_{fr}:

$$l = cm^{1/D_{fr}} \tag{22}$$

For aggregates of constant density, D_{fr} is 3 and Eq. 22 could express the relationship between the radius and the volume of a sphere. However, aggregates may have D_{fr} values as low as 1.75 (Meakin, 1991). As a result, a given mass will have a much larger radius than a solid sphere with the same mass would. The standard way to measure the length of a fractal is to use the root mean-square radius, called the radius of gyration r_g. It is given by Tanford (1961)

$$r_g = \left(M^{-1} \sum_{k=1}^{i} m_k r_k^2 \right)^{0.5} \tag{23}$$

where M is the total aggregate mass, m_k and r_k are the mass and distance from the center of mass of the k-th subparticle in the aggregate, and i is the total number of such subparticles. If all of the subparticles have the same mass, then Eq. 23 reduces to

$$r_g = \left(i^{-1} \sum_{k=1}^{i} r_k^2 \right)^{0.5} . \tag{24}$$

The values of c and D_{fr} depend on the system. If the aggregates are not porous, D_{fr} is 3. Values of D_{fr} have been estimated for marine systems that range from 1.26 to 2.49 (*e.g.*, Logan and Wilkinson 1990, Li and Logan 1995, Jackson *et al.*, 1995). Smaller values of D_{fr} usually indicate more porous structures.

The size spectrum has been extended to two dimensions using fractal scaling in Jackson (1998) and applied to a marine food web using multiple types of particles in Jackson (2001).

6.0.3 Models of bloom dynamics incorporating coagulation

The simplest phytoplankton growth/coagulation model assumed that single cells formed the basis for the system, that they were dividing at a constant specific growth rate μ, and that the ultimate fate for any particle was to sediment out of the mixed layer (Jackson, 1990):

$$\begin{aligned} \frac{dn_1}{dt} &= \mu n_1 - \alpha n_1 \sum_{i=1}^{\infty} n_i \beta_{1i} - n_1 v_1 Z^{-1} \\ &= + \text{ growth } - \text{ coagulation loss } - \text{ sedimentation} \end{aligned} \tag{25}$$

$$\begin{aligned} \frac{dn_i}{dt} &= 0.5\alpha \sum_{j=1}^{i-1} n_j n_{i-j} \beta_{j,i-j} - \alpha n_i \sum_{j=1}^{\infty} n_j \beta_{ij} - n_i v_i Z^{-1} \qquad \text{for } i \neq 1 \\ &\quad + \text{ coagulation gain } - \text{ coagulation loss } - \text{ sedimentation} \end{aligned} \tag{26}$$

where Z is the depth of the surface mixed layer, v_i is the settling velocity for a particle of type i, and, as noted earlier, $E_{ij} = \alpha$. (Note that these equations differ from those of Jackson (1990), in which the β_{ij} term was erroneously multiplied by a factor $(\delta_{ij} + 1)$. The result is that those calculations erroneously doubled the loss rate for collisions between similar particles.)

Results showed that there was a maximum concentration that solitary algal cells could have. This maximum was determined by a balance between the formation of new cells by division and the loss of single cells to aggregates and, ultimately, to settling out of the mixed layer. The maximum concentration could be estimated by assuming that it happened at steady state and that all of the single

cell aggregation was caused by collision with other single cells. This simplification was the result of an assumption that collisions with aggregates were negligible, which simulations showed to be true. It also neglected any non-algal particles which could be important in natural situations (Hill, 1992). The resulting estimate of the maximum concentration n_{cr}, was:

$$n_{cr} = 0.10(\mu - v_1/Z)(\alpha\gamma)^{-1} r_1^{-3} \tag{27}$$

n_{cr} is a function only of shear coagulation because Brownian coagulation was assumed to be insignificant for particles > 1 μm and because there are no collisions between two identical cells falling at the same speed. (Note that the result in Jackson (1990) is half that of Eq. 27 because of the error noted above.)

A more sophisticated model included the dependence of algal growth on environmental factors by making the growth rate a function of nutrient concentration and light intensity (Jackson and Lochmann, 1992). Expressed in the continuous particle size distribution form (see Eq. 21), the growth equations become:

$$\begin{aligned} \frac{dn(m,t)}{dt} &= \mu n - nvZ^{-1} \\ &\quad + \frac{1}{2}\int_0^m \alpha(m_1, m-m_1)\beta(m_1, m-m_1)n(m_1,t)n(m-m_1,t)dm_1 \\ &\quad - n(m,t)\int_0^\infty \alpha(m,m_1)\beta(m,m_1)n(m_1,t)dm_1 \end{aligned} \tag{28}$$

where m is the particle mass.

This can be re-formulated in sections, each section spanning a range with its upper limit twice its lower limit. (Jackson and Lochmann, 1992; Gelbard *et al.*, 1980) While not required, the ratio of the upper to lower masses in a section being two makes the computation of sectional coagulation coefficients simpler (Gelbard *et al.*, 1980). These equations can be numerically integrated in conjunction with equations determining the light attenuation, nitrate concentration, and their relationship to μ for different initial values of nitrate, mixed layer depth, algal size, and shear rates. Solitary algae are no longer monodisperse but are distributed over the sectional mass range, with the mass of smallest alga being half that of the largest.

This second model for algal growth coagulation has shown two dominant effects.

As in the first model, losses of single cells to aggregates can occur at a rate great enough to balance the formation of new cells by algal division. The parameter n_{cr} remains a useful estimate for this situation. Second, even for situations where the coagulation rate does not limit the maximum algal concentration, coagulation can enhance the loss of algal material from the surface layer.

Efforts to test the concept of critical concentration have been amazingly successful. Kiørboe *et al.* (1994) found that a simple extension of the concept successfully the maximum concentrations of algae during a successional spring bloom in a Danish fjord.

Tiselius and Kuylenstierna (1996).

Table 1: Notation for coagulation model.

Symbol	Description Values		Dimensions
m	Particle mass	–	g
m_i	Particle mass for upper bound of ith section	–	g
m_0	Particle mass of smallest particle	–	g
n	Particle number spectrum	–	# cm^{-4}
n_i	Particle number spectrum in ith section	–	# cm^{-4}
r	Particle radius	–	cm
Q_k	Concentration of mass in particles in k section	–	g cm^{-3}
s	Total number of sections	–	–
v, w	Particle settling rate	–	cm s^{-1}
V	Conserved particle volume	–	cm^3
Z	Mixed layer depth	–	m
${}^1\bar{\beta}_{i,j}$, ${}^2\bar{\beta}_{i,j}$, ${}^3\bar{\beta}_{i,j}$, ${}^4\bar{\beta}_{i,j}$, ${}^5\bar{\beta}_{i,j}$	Sect coefficients for reactions to-fro j sect	–	***
a, b	Constants for $n(r)$		cm^{-4+b}

7 Background: using the sectional approach to solve the coagulation equations

To find out how the particle distribution evolves with time and to find steady state particle distributions, the coagulation equation (Eq. 21) must be solved. This can be done by taking a geometrical sectional approach (Gelbard *et al.*, 1980; Jackson and Lochmann, 1992; Jackson, 1995). The range of particle masses being considered is divided into contiguous size ranges (sections) such that the particle mass at the upper bound of a section is twice that at its lower bound. The particle number spectrum is assumed to consist of a time varying part and a part which varies with the particle size:

$$n_m(m,t) = \frac{Q_l(t)}{m m_{l-1}} \tag{29}$$

where the particle mass m lies between the upper, m_l, and lower, m_{l-1}, bounds on the section l and Q_l is the total particulate mass of particles with $m_l > m > m_{l-1}$.

Gelbard *et al.* (1980) and Jackson and Lochmann (1992) show that using Eq. 29 in Eq. 21 results in the following equation for $m_{i+1} = 2m_i$

$$\begin{aligned}
\alpha^{-1}\frac{dQ_k}{dt} &= Q_{k-1}\sum_{i=1}^{k-1} {}^1\bar{\beta}_{i,k}Q_i && \text{gain from collision } i,\ k-1 \\
&\quad + Q_k\sum_{i=1}^{k-1} {}^2\bar{\beta}_{i,k}Q_i && \text{gain from collision } i,\ k \\
&\quad - Q_k\sum_{i=1}^{k-1} {}^3\bar{\beta}_{i,k}Q_i && \text{loss from collision } i<k,\ k \\
&\quad - {}^4\bar{\beta}_{k,k}Q_k^2 && \text{loss from collision } i=k,\ k \\
&\quad - Q_k\sum_{i=k+1}^{s} {}^5\bar{\beta}_{i,k}Q_i && \text{loss from collision } i>k,\ k \\
&\quad - \frac{Q_k}{Z\alpha m_{k-1}}\int_{m_{k-1}}^{m_k} w(m)\,dm && \text{loss to settling out of mixed layer}
\end{aligned} \tag{30}$$

Table 2: Definition of sectional coagulation coefficients. These have been derived from those of Gelbard et al (1980) for the case of mass conservation.

Symbol	Range	Value
${}^1\beta_{ijl}$	$i < l-1,\ j < l-1,\ 2 \le l \le s$	0
	$i \le l-1,\ j = l-1,\ 2 \le l \le s$	$\frac{1}{m_{i-1}m_{l-2}} \int_{m_{i-1}}^{m_i} \int_{m_{l-1}-\overline{m}_1}^{m_{l-1}} \frac{(\overline{m}_1+\overline{m}_2)\beta(\overline{m}_1,\overline{m}_2)}{\overline{m}_1\overline{m}_2} d\overline{m}_2 d\overline{m}_1$
	$i = l-1,\ j = l-1,\ 2 \le l \le s$	$\frac{1}{2m_{l-2}^2} \int_{m_{l-2}}^{m_{l-1}} \int_{m_{l-2}}^{m_{l-1}} \frac{(\overline{m}_1+\overline{m}_2)\beta(\overline{m}_1,\overline{m}_2)}{\overline{m}_1\overline{m}_2} d\overline{m}_2 d\overline{m}_1$
${}^2\bar{\beta}_{ijl}$	$i < l,\ j = l,\ 2 \le l \le s$	$\frac{1}{m_{i-1}m_{l-1}} \int_{m_{i-1}}^{m_i} \int_{m_l-\overline{m}_1}^{m_l} \frac{\beta(\overline{m}_1,\overline{m}_2)}{\overline{m}_1} d\overline{m}_2 d\overline{m}_1$
		$-\frac{1}{m_{i-1}m_{l-1}} \int_{m_{i-1}}^{m_i} \int_{m_{l-1}}^{m_l-\overline{m}_1} \frac{\beta(\overline{m}_1,\overline{m}_2)}{\overline{m}_2} d\overline{m}_2 d\overline{m}_1$
${}^3\bar{\beta}_{ijl}$	$i = j = l, 1 \le l \le s$	$\frac{1}{2m_{l-1}^2} \int_{m_{l-1}}^{m_l} \int_{m_{l-1}}^{m_l} \frac{(\overline{m}_1+\overline{m}_2)\beta(\overline{m}_1,\overline{m}_2)}{\overline{m}_1\overline{m}_2} d\overline{m}_2 d\overline{m}_1$
${}^4\bar{\beta}_{ijl}$	$l < i, j = l, 1 \le l \le s$	$\frac{1}{m_{i-1}m_{l-1}} \int_{m_{i-1}}^{m_i} \int_{m_{l-1}}^{m_l} \frac{\beta(\overline{m}_1,\overline{m}_2)}{\overline{m}_1} d\overline{m}_2 d\overline{m}_1$

where s is the total number of sections used in the simulation, ${}^1\bar{\beta}_{i,k}$, ${}^2\bar{\beta}_{i,k}$, ${}^3\bar{\beta}_{i,k}$, ${}^4\bar{\beta}_{i,k}$, ${}^5\bar{\beta}_{i,k}$ are the sectional coagulation coefficients defined according to Gelbard *et al.*(1980) for the indicated ranges and α has been assumed to be constant.

8 References

Alldredge, A. L., U. Passow, and B. E. Logan. 1993. The abundance and significance of a class of large, transparent organic particles in the ocean. Deep-Sea Research, **40**, 1131-1140.

Adler, P. M. 1981. Interaction of unequal Spheres. I. hydrodynamic interaction: colloidal forces, J. Colloid Interface Sci. 84: 461-474.

Batchelor, G. K., and J. T. Green. 1972. The hydrodynamic interaction of two small freely-moving spheres in a linear flow field, J. Fluid. Mech. 56: 375–400.

Delichatsios, M.A., and R. F. Probstein. 1975. Coagulation in turbulent flow: theory and experiment. J. Colloid Interface Sci. 51: 394–405.

Friedlander, S. K. 1977. Smoke, dust and haze. Wiley.

Gelbard, F., Y. Tambour, and J. H. Seinfeld. 1980. Sectional representations for simulating aerosol dynamics. J. Coll. Interface Sci., 76: 541-556.

Figure 10: Example of different ways of representing particle size spectrum using sectional approach. Results are from a calculation made using the **simple** program suite. Conserved volume is used in place of mass. Left: values of Q_i as a function of section number i; middle: the equivalent size spectrum $n(m)$ (as a function of mass); right: the same equivalent size spectrum as a function of radius r ($n(r)$).

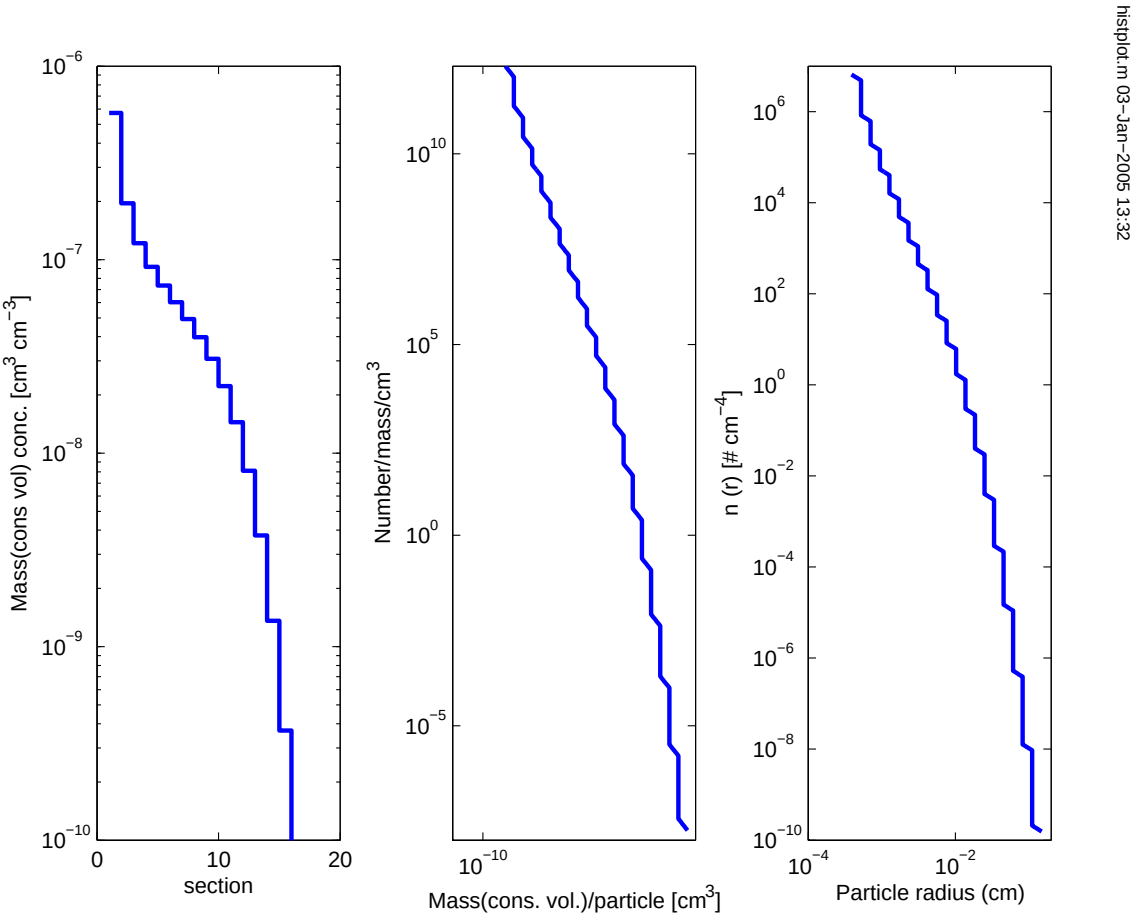

Han, M., and D. F. Lawler. 1991. Interactions of two settling spheres: settling rates and collision efficiency, *J. Hydraul. Eng.* 117: 1269-1289.

Han, M., Lawler, D. F., 1992. The (relative) insignificance of G in flocculation. Journal of the American Water Works Association 84(10), 79-91.

Hill, P. S. 1992. Reconciling aggregation theory with observed vertical fluxes following phytoplankton blooms. J. Geophy. Res., 97: 2295–2308.

Hill, P. S., A. R. M. Nowell, and P. A. Jumars. 1992. Encounter rate by turbulent shear of particles similar in diameter to the Kolmogorov scale. J. Mar. Res. 50: 419-446.

Jackson, G. A. 1990. A model of the formation of marine algal flocs by physical coagulation processes. Deep-Sea Res. 37: 1197–1211.

Jackson, G. A. 1993. Flux feeding as a mechanism for zooplankton grazing and its implications for vertical particulate flux. Limnol. Oceanogr. 38: 1328–1331.

Jackson, G. A. 1995. TEP and coagulation during a mesocosm experiment. Deep-Sea Res. II. 42: 215– 222.

Jackson, G. A. 1998. Using fractal scaling and two dimensional particle size spectra to calculate coagulation rates for heterogeneous systems. J. Colloid Interface Sci. **202**: 20-29.

Jackson GA (2001) Effect of coagulation on a model planktonic food web. Deep-Sea Res I 48: 95–123

Jackson, G. A. and S.E. Lochmann. 1992. Effect of coagulation on nutrient and light limitation of an algal bloom. Limnol. Oceanogr., 37: 77–89.

Jackson G. A., Maffione R, Costello DK, Alldredge AL, Logan BE, Dam HG (1997) Particle size spectra between 1 μm and 1 cm at Monterey Bay determined using multiple instruments. Deep-Sea Res I 44 (11): 1739–1767

Kao, W.V., R. G. Cox, and S. G. Mason. 1977. Streamlines around single spheres and trajectories of pairs of spheres in two-dimensional creeping flows, Chem. Eng. Sci. 32: 1505-1515.

Kiørboe, T., K. P. Andersen, and H. G. Dam. 1990. Coagulation efficiency and aggregate formation in marine phytoplankton. Mar. Biol. **107**, 235-245 .

Kiørboe, T. P., and J. L. S. Hansen. 1993. Phytoplankton aggregate formation: observations of patterns and mechanisms of cell sticking and the significance of exopolymeric material. J. of Plankton Res., **15**, 993-1018.

Kiørboe, T. P., C. Lundsgaard, M. Olesen, and J. L. S. Hansen. 1994. Aggregation and sedimentation processes during a spring phytoplankton bloom: a field experiment to test coagulation theory. J. Mar. Res., **52**, 297-323.

Li, X. and B. E. Logan (1995) Size distributions and fractal properties of particles during a simulated phytoplankton bloom in a mesocosm. *Deep-Sea Research II*, **42**, 125–138.

Li, X., Logan, B. E., 1997. Collision frequencies of fractal particles with small particles by differential sedimentation. Environmental Science and Technology 31, 1229-1236.

Li, X., Logan, B. E., 1997a. Collision frequencies between fractal aggregates and small particles in a turbulently sheared fluid. Environmental Science and Technology 31, 1237-1242.

Logan, B. E., and D. B. Wilkinson (1990) Fractal geometry of marine snow and other biological aggregates, Limnol. Oceanogr., **35**, 130–136

Logan, B. E., U. Passow, A. L. Alldredge, H. P. Grossart, and M. Simon. 1995. Rapid formation and sedimentation of large aggregates is predictable from coagulation rates (half-lives) of transparent exopolymer particles (TEP). Deep-Sea Res. II. 42: 203–214.

McCave, I. N. 1984. Size spectra and aggregation of suspended particles in the deep ocean. Deep-Sea Res., **31** 329-352.

Meakin, P. 1991. Fractal aggregates in geophysics, Rev. Geophys. 29: 317- 354 .

O'Melia, C. R. 1972. An approach to modeling of lakes. Schweiz. Z. Hydrol., **34**, 1-33.

Poe, G. G., and A. Acrivos. 1975. Closed-streamline flows past rotating single cylinders and spheres: inertia effects. J. Fluid Mech. 72: 605-623.

Pruppacher, H. R. and J. D. Klett. 1980. Microphysics of clouds and precipitation. Riedel.

Saffman, P.G., and J. S. Turner. 1956. On the Collision of Drops in Turbulent Clouds, *J. Fluid Mech.* 1: 16-30.

Serra, T., and Logan, B. E. 1999. Collision frequencies of fractal bacterial aggregates with small particles in a sheared fluid. Environmental Science and Technology 33, 2247-2251.

Stumm, W., and J. J. Morgan. 1995. Aquatic chemistry, 3rd ed. Wiley.

Tanford, C. 1961 *Physical Chemistry of Macromolecules.* (New York: John Wiley and Sons)

Tiselius, P., and M. Kuylenstierna. 1996. Growth and decline of a diatom spring bloom: phytoplankton species composition, formation of marine snow and the role of heterotrophic dinoflagellates. J. Plankton Res. 18: 133-155.

Vicsek, T., 1992. Fractal growth phenomena, 2nd ed. World Scientific, Singapore, 1992.

Witten, T. A., and M. E. Cates. 1986. Tenuous structures and disorderly growth processes, Science. 232:1607-1612.